JOURNAL OF GEOPHYSICAL RESEARCH, VOL. 94, NO. A1, PAGES 443–452, JANUARY 1, 1989

Coherent Cerenkov Radiation From the Spacelab 2 Electron Beam

W. M. FARRELL, D. A. GURNETT, AND C. K. GOERTZ

Department of Physics and Astronomy, University of Iowa, Iowa City

During the Spacelab 2 mission, a spacecraft called the Plasma Diagnostics Package (PDP) was released from the space shuttle to investigate the surrounding plasma environment. During an interval when the shuttle and PDP were magnetically connected, a continuous 1-keV/50-mA electron beam was ejected along a field line from an electron generator on board the shuttle. As the PDP flew by the beam, the PDP plasma wave instrument detected intense whistler mode radiation originating from the beam. It is believed that coherent Cerenkov radiation from bunches of beam electrons is responsible for the whistler mode radiation, where an electrostatic beam-plasma instability forms the coherently radiating bunches. In this paper a detailed model of the coherent Cerenkov emission process is presented. A one-dimensional computer simulation of the beam is used to model the expected phase space structure of the electrons, and power emitted from Cerenkov radiation is computed using an analytical expression. The calculated power from the modeled 200-m beam segment is $\sim 5 \times 10^{-8}$ W/Hz, which can easily account for the measured whistler mode wave power. The inclusion of coherent effects in the beam increases the wave powers by nearly 90 dB above incoherent power levels. These calculations demonstrate that a spontaneous emission process, alone, can account for the observed whistler mode wave powers.

1. INTRODUCTION

During the Spacelab 2 (SL 2) mission, intense whistler mode radiation from an electron beam ejected from the space shuttle was detected by radio receivers on board the Plasma Diagnostics Package (PDP) which was in free flight around the shuttle [*Gurnett et al.*, 1986]. Simple calculations have indicated that coherent Cerenkov radiation emitted by bunches of beam electrons may produce such whistler mode signals [*Bell*, 1968; *Farrell et al.*, 1988], with the bunches being formed by a beam-plasma instability. This paper presents a detailed model of this wave generation process, including a determination of the expected radiated power.

In July of 1985, the space shuttle carried the SL 2 payload into the upper ionosphere. One of the experiments on board was the University of Iowa's Plasma Diagnostics Package, which contained 10 experiments designed to study the plasma environment around the shuttle orbiter. Another experiment, the Vehicle Charging and Potential Experiment (VCAP), also flew on the mission to study the charging and potential of the shuttle. Part of this package included a fast pulsed electron generator (FPEG) designed to eject a 1-keV/50-mA electron beam.

The PDP was released from the shuttle for a 6-hour period on August 1, 1985, to investigate the plasma environment in an extended region around the shuttle. At specific times the PDP intersected geomagnetic field lines that connected to the shuttle orbiter. These times are known as magnetic conjunction. During one magnetic conjunction event, the FPEG, located in the shuttle cargo bay, continuously ejected a 1-keV/50-mA electron beam with a pitch angle that varied from 0° to 20°. The PDP, located 200 m from the shuttle, passed within 6 m of the magnetic flux tube containing the beam. During this magnetic conjunction, the PDP plasma wave instrument detected intense whistler mode radiation. Figure 1 displays a frequency-versus-time spectrogram from the PDP plasma wave instrument during the 1-keV/50-mA beam ejection (0330–0337 UT). The whistler mode emission is the funnel-shaped structure extending in frequency from about 30 kHz to about 1 MHz.

Whistler mode signals like those detected during the SL 2 beam ejection are commonly detected from both artificially and naturally created electron beams in the Earth's ionosphere. In particular, rocket-launched electron beam experiments performed in the 1970s clearly showed the occurrence of whistler mode radiation in association with injected electron beams (*Cartwright and Kellogg* [1974], *Monson et al.* [1976], and *Dechambre et al.* [1980], just to name a few). With the advent of the shuttle program, these experiments were continued at a new level of sophistication which was due, in part, to the diagnostics packages, such as the PDP, that could be placed in favorable positions relative to the ejected electron beams. During beam ejections from the shuttle, many strong LF and VLF emissions were detected [*Shawhan et al.*, 1984; *Beghin et al.*, 1984; *Neubert et al.*, 1986], including intense whistler mode radiation [*Gurnett et al.*, 1986; *Farrell et al.*, 1988]. For a comprehensive review of the many wave modes excited by artificially generated electron beams, see *Grandel* [1982]. Besides artificial beams, whistler mode radiation called auroral hiss is also emitted from field-aligned electron beams that occur naturally in the auroral regions [*Gurnett*, 1966; *Lin et al.*, 1984]. Like the whistler mode radiation detected from the SL 2 electron beam, these emissions appear funnel shaped on a radio spectrogram. It has been demonstrated that this shape results from a propagation effect of whistler mode waves with normal angles near the resonance cone [see *Gurnett*, 1983]. Based on the striking similarities between auroral hiss and the whistler mode radiation from the SL 2 electron beam, further investigation of the latter was performed.

In particular, the whistler mode emission from the 1-keV/50-mA SL 2 electron beam has been the subject of two studies [*Gurnett et al.*, 1986; *Farrell et al.*, 1988]. Evidence presented in both indicates that the emission is quasi-electrostatic and is propagating with wave normals near the resonance cone. The emission is also believed to be generated by a Landau resonance interaction, since its index of refrac-

Paper number 88JA03335.
0148-0227/89/88JA-03335$05.00

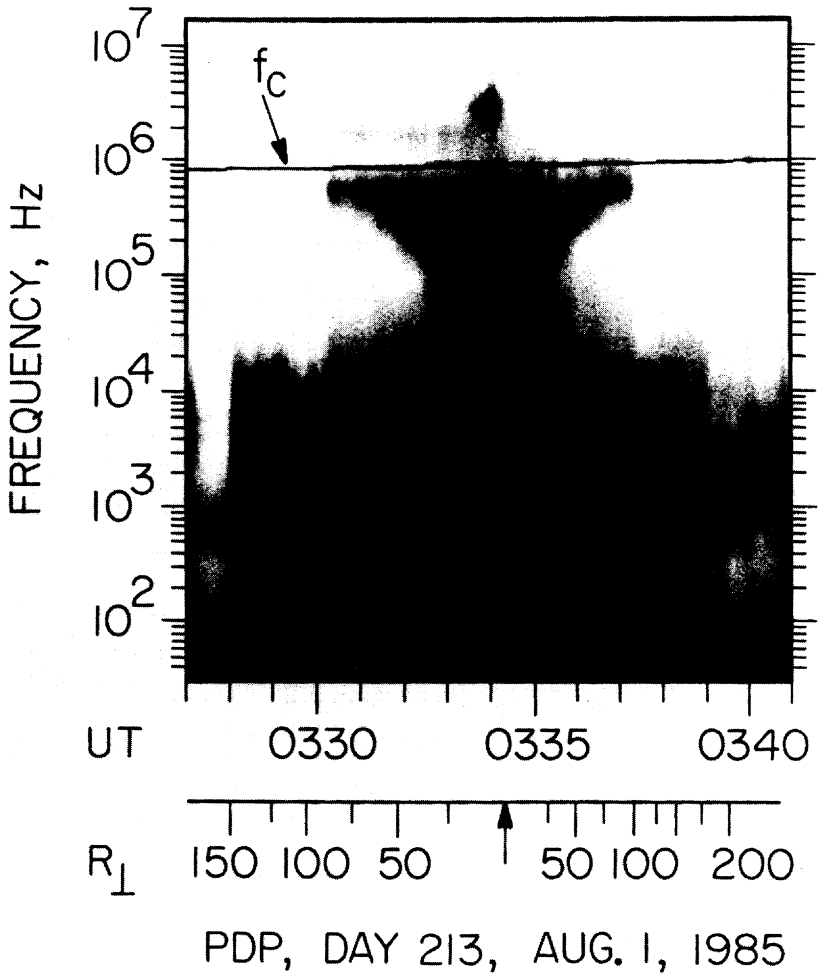

Fig. 1. Frequency versus time spectrogram from the PDP plasma wave instrument showing intense emissions during a continuous electron beam event (0330–0337 UT). The funnel-shaped structure that extends from the electron cyclotron frequency f_c to about 30 kHz is whistler mode radiation from the beam.

tion values are near those expected for such an interaction [*Farrell et al.*, 1988] and $k \cdot v_b > 0$ [*Gurnett et al.*, 1986]. The radiated whistler mode power from the first 200 m of the beam was calculated by integrating the Poynting flux through a surface that contained the PDP trajectory [*Farrell et al.*, 1988]. The resulting power spectrum is displayed in Figure 2. Note that the power spectral density, dP/df, is $\sim 10^{-9}$ W/Hz. The total power radiated in the whistler mode from the 200-m beam segment has been estimated to be 1.6 mW, which corresponds to a linear emissivity of about 8×10^{-6} W/m. Since the total power in the beam is 50 W, the beam converted only 3.2×10^{-5} of its power to whistler mode radiation in the first 200 m of its trajectory.

Owing to the low efficiency of converting beam power to wave power, incoherent Cerenkov radiation from the beam electrons was initially considered as the source of the emission. However, the estimated power from this radiation process is 10^7 times smaller than that detected [*Farrell et al.*, 1988]. In reality, the beam cannot be considered an incoherent radiator since a beam-plasma instability is operating in the beam forming quasi-periodically spaced density perturbations or "bunches" which can radiate coherently. Therefore an emission process involving coherent Cerenkov radiation from these bunches was considered [*Farrell et al.*, 1988]. Strong instability-related electrostatic turbulence near the local plasma frequency, f_{pe}, was detected in the beam by the PDP plasma wave instrument. These waves interact with the beam and form the "bunches" which can spontaneously emit powerful Cerenkov radiation due to the increased coherence of the beam electrons. The Cerenkov radiation emitted from these coherent structures is then detected by the PDP plasma wave receiver as the whistler mode radiation. As demonstrated previously [*Farrell et al.*, 1988], the frequency range of the emitted Cerenkov radiation closely corresponds to that of the detected whistler mode radiation, and the bunching may create enough coherence among the beam electrons to yield the measured wave powers.

In this paper we will present a model of the coherent Cerenkov radiation from a bunched electron beam like that on the SL 2 experiment. We note that there are other possible mechanisms for generating the whistler mode radiation, such as a whistler mode instability in the beam [*Lin and Wong*, 1988] or some nonlinear mode conversion process. However, we will only consider the coherent Cerenkov radiation model and attempt to demonstrate that this process alone can account for the measured wave powers. In section 2 an expression is derived that describes the coherent Cerenkov radiated power from a field-aligned electron beam. This expression

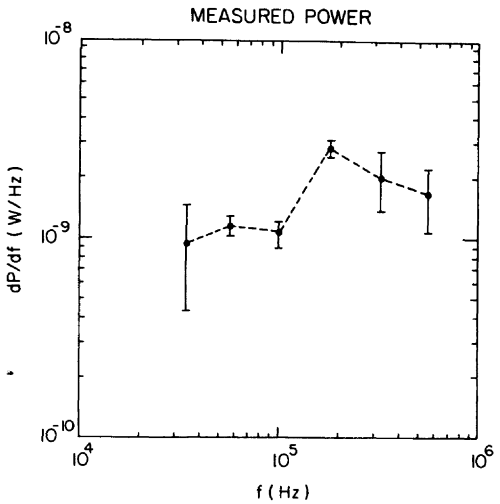

Fig. 2. Calculated power spectral density from the first 200 m of the beam in the whistler mode as a function of frequency.

will be applied to a model of the SL 2 electron beam obtained from a one-dimensional particle simulation, the results of which are outlined in section 3. In section 4, the power from the modeled beam is calculated and compared with the measured power in the whistler mode from the actual SL 2 electron beam.

2. Expression for the Radiated Power

In this section an expression is derived for the power emitted from an electron beam by a coherent Cerenkov radiation process. The derivation presented here is similar to that of *Mansfield* [1967], who calculated the radiated power from a single test particle in a plasma medium using the Fourier transforms of the source current and radiated electric field. Using a similar analytical technique, *Harker and Banks* [1983] derived an expression for the power radiated from a pulsed electron beam in a plasma medium which included coherent effects between the radiating electrons in the pulses. In their derivation it was assumed that all beam electrons traveled with the same velocity $\bar{v}$ in pulses of length l with a distance d separating each pulse and that the pulsing is imposed by the generator that produces the beam. Compared with the incoherently radiated power from a beam, the inclusion of coherent effects between radiating beam electrons in a pulse leads to much higher powers. The calculations performed in our analysis are similar to theirs, except that we are now considering the radiation from an initially continuous beam that becomes modulated or "bunched" owing to the beam-plasma instability.

In the derivation of the radiated power presented here, it is assumed that the beam is a line source radiator of electromagnetic radiation. This assumption is valid since the whistler mode wavelength λ_{em} is of the order of 20 m and is several times greater than the beam diameter d, which is at most 2 cyclotron radii or about 6 m [*Farrell et al.*, 1988]. As will soon be demonstrated, this assumption will allow the current from the field-aligned SL 2 electron beam to be adequately represented by a delta function.

We also assume that the beam electrons only act as test particles which do not significantly alter the ambient plasma medium. Consequently, the medium is represented by a homogeneous, cold, collisionless plasma in a static magnetic field, and the terms in the dielectric tensor $\bar{K}$ describing the beam are not included. Very near the electron generator this assumption is probably not valid, since the SL 2 electron beam is overdense ($n_b > n_a$), and thus the beam-related terms in $\bar{K}$ cannot be ignored. However, as pictures of shuttle-launched beams indicate [*Banks and Raitt*, 1988], the beams tend to expand and become tenuous as they propagate from their source. *Gendrin* [1974] has demonstrated that this expansion will cause an initially overdense beam to become underdense within a few meters from the point of injection, and it is in the underdense region where the test particle assumption is considered valid. From Banks and Raitt the expansion of a 1-keV/100-mA electron beam with an initial density of $n_b \cong 100n_a$ is about 13°. At this expansion rate the average beam density can become less than that of the ambients with the first meter (or $100\lambda_D$) of the injection point. Note that the beam expands from the generator opening of a couple centimeters to at most 1–2 cyclotron radii [*Gendrin*, 1974; *Banks and Raitt*, 1988] and is never larger than the whistler mode wavelength. Consequently, the assumption of a line source radiator still applies even though the beam diameter is increasing.

We write the equation for a wave in a cold plasma including the external current source, $\bar{J}_q(\bar{k}, \omega)$, as

$$\mathsf{T} \cdot \bar{E}(\bar{k}, \omega) = \frac{i\bar{J}_q(\bar{k}, \omega)}{\omega\varepsilon_0} \tag{1}$$

where $\mathsf{T} \cdot \bar{E}(\bar{k}, \omega) = \bar{n} \times \bar{n} \times \bar{E}(\bar{k}, \omega) + \mathsf{K} \cdot E(\bar{k}, \omega)$ and K is the cold plasma dielectric tensor. The form of the dielectric tensor used here can be found in the work of *Mansfield* [1967]. The electric field, $\bar{E}(\bar{r}, t)$, is obtained by taking the inverse Fourier transform of $\bar{E}(\bar{k}, \omega)$,

$$\bar{E}(\bar{r}, t) = \frac{1}{\varepsilon_0} \iint \mathsf{T}^{-1} \cdot \bar{J}_q(\bar{k}, \omega) e^{i(\omega t - k \cdot r)}\, d\bar{k}\, \frac{d\omega}{\omega} \tag{2}$$

The current density can be expressed in a generalized form for a line source as

$$\bar{J}_q(\bar{r}, t) = [\hat{x}J_x(x, t) + \hat{y}J_y(y, t) + \hat{z}J_z(z, t)] \cdot \delta(x - R_c \cos \omega_c t)\delta(y - R_c \sin \omega_c t) \tag{3}$$

where the beam displacement is

$$r = \hat{x}R_c \cos \omega_c t + \hat{y}R_c \sin \omega_c t + \hat{z}z \tag{4}$$

and R_c and ω_c are the cyclotron radius and frequency, respectively. The Fourier transform of this current is

$$\bar{J}_q(\bar{k}, \omega) = \frac{1}{(2\pi)^4} \int \bar{J}_q(\bar{r}, t) e^{i(\bar{k} \cdot \bar{r} - \omega t)}\, dr\, dt$$

$$= \frac{1}{(2\pi)^4} \int [\hat{x}J_x(x, t) + \hat{y}J_y(y, t) + \hat{z}J_z(z, t)] \cdot e^{i(k_z z - \omega t)} (e^{ik_x R_c \cos\omega_c t})(e^{ik_y R_c \sin\omega_c t})\, dz\, dt \tag{5}$$

The exponential factors in the parentheses can be reexpressed as

$$e^{ik_x R_c \cos\omega_c t} = \sum_{s=-\infty}^{\infty} J_s(k_x R_c) e^{-is\omega_c t}$$

and

$$e^{ik_y R_c \sin\omega_c t} = \sum_{s'=-\infty}^{\infty} J_{s'}(k_y R_c) e^{is'\omega_c t} \tag{6}$$

where J_s is the s order Bessel function. Inserting these into (5) yields the following expression for the transformed current:

$$\overline{J_q}(\bar{k}, \omega) = \frac{1}{(2\pi)^4} \int (\hat{x}J_x(x, t) + \hat{y}J_y(y, t) + zJ_z(z, t))e^{i(k_z z - \omega t)} \cdot \left[\sum_{s=-\infty}^{\infty} J_s(k_x R_c)e^{-is\omega_c t}\right]\left[\sum_{s'=-\infty}^{\infty} J_s(k_y R_c)e^{is'\omega_c t}\right] dz\, dt \quad (7)$$

During the SL 2 beam firing, the beam pitch angle was at most 20°, and for a 3-min period, from 0332:30 to 0335:30 UT, it was less than 10°. As a consequence, $V_{\parallel} \gg V_{\perp}$, which implies that $J_z(z, t) \gg J_x(x, t)$ and $J_y(y, t)$. Also, $R_c = V_{\perp}/\omega_c \ll \lambda_{em}$ and, therefore, the factors in the brackets in (7) are near unity. Equation (7) then becomes

$$\bar{J}_q(\bar{k}, \omega) = \frac{\hat{z}}{(2\pi)^4} \iint J_z(z, t)e^{i(k_z z - \omega t)}\, dz\, dt \quad (8)$$

Consider a group of particles ejected from a particle generator. Ideally, if all the particles are moving at the same velocity, V_s, a simple transformation can be made to a frame moving with the particles, $z' = z - V_s t$. In this frame the current density does not depend explicitly on time,

$$J_z(z, t) = J_z(z') \quad (9)$$

and consequently, the beam particles appear stationary. In order to solve the time integral in (8), a transformation to z' is made where the current density is considered time independent. In reality, it is not expected that all particles have identical velocities (i.e., they may have a spread ΔV about V_s), and the validity of the power expression derived assuming (9) must be established for the particular case in question.

Assuming that a transformation can be made to a frame where (9) is valid, expression (8) becomes

$$\bar{J}_q(\bar{k}, \omega) = \frac{\hat{z}}{(2\pi)^4} \int_{-\infty}^{\infty} J_z(z')e^{ik_z z'}\, dz' \int_{-\infty}^{\infty} e^{i(k_z V_s - \omega)t}\, dt \quad (10)$$

The quantity $\int_{-\infty}^{\infty} J_z(z')e^{ik_z z'}\, dz' = (2\pi)^{1/2}J_z(k_z)$, where $J_z(k_z)$ is the Fourier transform of $J_z(z')$. Using the definition of the delta function, $\int_{-\infty}^{\infty} e^{i(k_z V_s - \omega)t}\, dt = 2\pi\, \delta(k_z V_s - \omega)$, and the fact that $k_z = n\omega \cos\theta/c$, (10) reduces to

$$\bar{J}_q(\bar{k}, \omega) = \frac{\hat{z}}{(2\pi)^3} [(2\pi)^{1/2}J_z(k_z)]\, \delta(n\omega \cos\theta\beta - \omega) \quad (11)$$

where $\beta = V_s/c$.

In order to determine the radiated electric field, (11) is substituted into (2) to obtain

$$\bar{E}(\bar{r}, t) = \frac{1}{(2\pi)^3\varepsilon_0} \iint (T^{-1} \cdot z)[(2\pi)^{1/2}J_z(k_z)] \cdot \delta(n\omega \cos\theta\beta - \omega)e^{i(\omega t - \bar{k}\cdot\bar{r})}\, d\bar{k}\, \frac{d\omega}{\omega} \quad (12)$$

Knowing the electric field and source current, an expression for the radiated power can now be found:

$$P(t) = \int \bar{E}(\bar{r}) \cdot \bar{J}(r)\, d\bar{r} = \frac{1}{(2\pi)^2\varepsilon_0} \iint (\hat{z} \cdot \mathsf{T}^{-1} \cdot \hat{z})\{(2\pi)J_z[k_z(n, \theta)]J_z^*[k_z(n, \theta)]\} \cdot \delta(n\omega \cos\theta\beta - \omega)e^{i(\omega - n\omega\cos\theta\beta)t} n^2\omega^2\, dn \sin\theta\, d\theta\, d\omega \quad (13)$$

where $n^2(\omega^3/c^3)\, dn \sin\theta\, d\theta\, d\phi$ has been substituted for the element $d\bar{k}$ and the trivial integration over ϕ has been performed. Integrating over θ, an integral of the form

$$I = \int f(x)\delta(Ax - B)\, dx = \frac{f(x_0)}{A}$$

must be solved, where $A = |n\omega\beta|$, $B = \omega$, and $x_0 = \cos\theta_0 = 1/n\beta$. It should be noted that to obtain a nonzero solution to the integral, the condition $\cos\theta_0 = 1/n\beta$ must be satisfied, which is the Landau resonance condition. Upon evaluating the integral, the radiated power becomes

$$P(t) = \frac{-i}{(2\pi)^2\varepsilon_0 c^3\beta} \iint (\hat{z} \cdot \mathsf{T}^{-1} \cdot \hat{z})\{(2\pi)J_z[k_z(n, \theta_0)] \cdot J_z^*[k_z(n, \theta_0)]\}|n|\,|\omega|\, dn\, d\omega \quad (14)$$

From Mansfield, the quantity $(\hat{z} \cdot \mathsf{T}^{-1} \cdot \hat{z})$ is

$$(\hat{z} \cdot \mathsf{T}^{-1} \cdot \hat{z}) = \frac{T_{33}(n)}{\varepsilon_1(n^2 - n_2^2)(n_2 - n_1^2)} \quad (15)$$

where

$$T_{33} = \varepsilon_1^2 - \varepsilon_2^2 - \varepsilon_1 n^2 + (n^4 - \varepsilon_1 n^2)\cos^2\theta_0 \quad (16)$$

$$n_{1,2}^2 = [-B \pm (B^2 - 4Ce_1)^{1/2}]/2\varepsilon_1 \quad (17)$$

$$B = \left(\frac{c}{V_s}\right)^2 (\varepsilon_3 - \varepsilon_1) + \varepsilon_2^2 - \varepsilon_1^2 - \varepsilon_1\varepsilon_3 \quad (18)$$

and

$$C = \left(\frac{c}{V_s}\right)^2 (\varepsilon_1^2 - \varepsilon_2^2 - \varepsilon_1\varepsilon_3) + \varepsilon_3(\varepsilon_1^2 - \varepsilon_2^2) \quad (19)$$

Using the Plemelj formula, the complex integration over dn is performed to yield the final expression for the radiated power:

$$P(t) = \bar{P} = \int_{-\infty}^{\infty} \left(\frac{\omega\, d\omega}{8\pi\varepsilon_0\varepsilon_1 c^2 V_s}\right) \frac{1}{(n_2^2 - n_1^2)} \sum_{k=1}^{2} T_{33}(n_k) \cdot \{2\pi J_z[k_z(n_k, \theta_0)]J_z^*[k_z(n_k, \theta_0)]\} \quad (20)$$

Note that the radiated power is proportional to the square of the Fourier transform of the current density. This result is similar to that obtained by *Harker and Banks* [1983], who found that the radiated power varies as the square of the transform of the current pulses. Once the current density and its transform are known, it can be used in (20) to easily calculate the radiated power. We will use a modeled beam to obtain the beam current, $J_z(z, t)$, since the available plasma instruments flown on the PDP cannot directly measure the electron bunching which occurs on time scales of $1/\omega_{pe} \sim 10^{-7}$ s. The results of the beam simulation are presented in the next section.

3. A One-Dimensional Electrostatic Simulation of the SL 2 Electron Beam

To obtain the required beam current, a one-dimensional electrostatic model of an electron beam propagating through an ambient plasma is simulated on a computer. A one-dimensional beam model was chosen, since the length scales being considered are very long, about 200 m (many thousand Debye lengths), and cannot be reasonably modeled using a two- or three-dimensional system owing to the practical limits on computer CPU time. In the one-dimensional model it is assumed that the velocity of the particles is directed along a

static magnetic field line, which allows the particle trajectories to be unaffected by this field. Since the SL 2 electron beam was nearly field aligned during injection, this assumption is acceptable. In this analysis we also assume that the magnitude of the electric field of the generated Cerenkov radiation is much smaller than that of the electrostatic wave generated within the beam, $E_{ES} \gg E_{RAD}$. This assumption implies that the radiated electric field did not significantly alter the SL 2 beam electron trajectories and is consistent with the modeling of the beam where radiation field effects are neglected. This assumption is also consistent with observations made during the SL 2 experiment, where $E_{ES} \geq 0.3$ V/m in the beam while $E_{RAD} \sim 10^{-3}$ V/m for the whistler mode waves.

The simulation is designed so that initially the system is charge neutral. The particles representing the ambient electrons can move freely; however, they are confined to the system by reinjection boundaries. Ambient electrons leaving the system at these boundaries are reinjected with a Gaussian-weighted velocity between zero and the electron thermal speed. The electron beam is represented by particles of negative charge that are injected into the system at the $z = 0$ boundary with velocities greater than the ambient electron thermal speed. In order to keep the net charge in the system equal to zero, a positive charge equal in magnitude to the amount of negative beam charge in the system is placed at the $z = 0$ boundary. This boundary charge draws a return flow of ambient electrons which, for low beam flux ($n_b V_b A < n_A V_A A$), is sufficient to keep the boundary almost completely neutralized.

In a one-dimensional simulation the particles are charged sheets of infinite extent in the transverse direction and of finite thickness ($\sim \lambda_D$) along the direction being modeled. Consequently, the modeled beam has an infinite cross section. This infinite cross-section model, however, is contrary to the true SL 2 electron beam, which had a cross-sectional radius of no more than 6 m [*Farrell et al.*, 1988]. Assuming such a model ignores finite radius electrostatic effects associated with the SL 2 electron beam and is only justified if the wavelength of the longitudinal electrostatic mode, λ_{ES}, is less than the SL 2 electron beam diameter d, which is not the case. Therefore we must demonstrate that the electrostatic nature of a finite radius beam, like the SL 2 electron beam, is similar to that of an infinite radius beam. To show this, a comparison will be made between our one-dimensional beam model and a two-dimensional radially finite beam model [*Winglee and Pritchett*, 1988] to verify such similarities.

Figure 3 displays a beam phase space configuration from *Winglee and Pritchett*'s [1988] two-dimensional simulation of a radially finite beam. In their simulation an initially overdense beam is injected into a model ionosphere, with the ratio of the beam density to ambient density, n_b/n_A, equal to 4 and beam velocity to ambient thermal velocity, V_b/V_{TH}, equal to 20. Both ratios used in the simulation are representative of the conditions during SL 2 electron beam injections. From this figure we see that the beam can freely propagate from the injection boundary (located at $x/\Delta = 125$). In this case, the spacecraft charging potential at the injection boundary is much less than the initial beam energy, $\phi < \frac{1}{2} m_e V_b^2$, and will allow the beam to escape from the near-injection region. This low spacecraft potential is consistent with potential measurements made during the SL 2 mission where the shuttle obtained only a 40-V potential during ejections of a 1-keV electron beam [*Williamson et al.*, 1985; *Hawkins et al.*, 1987]. As

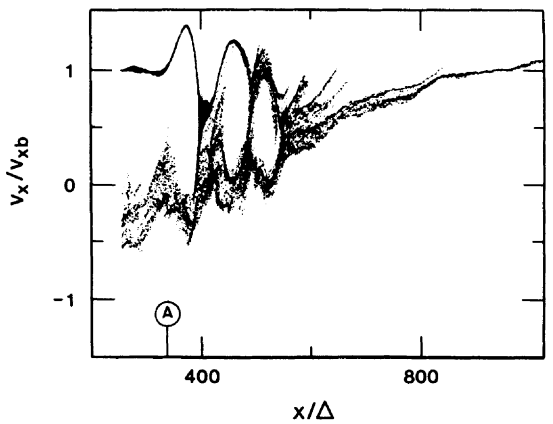

Fig. 3. Phase space configuration of beam electrons from *Winglee and Pritchett*'s [1988] two-dimensional simulation. In this model the beam is initially injected overdense ($n_b/n_A = 4$). The ratio $V_b/V_A = 20$ and the figure displays the beam phase space after about $38\omega_{pe}^{-1}$. Note that the wave-trapping structures created in the beam are very similar to those typically created in one-dimensional simulations of underdense beams.

can be seen in the figure, the classic trapping structures created in this beam are very similar to those obtained in one-dimensional simulations [*Okuda et al.*, 1987; *Okuda and Kan*, 1987; *Winglee et al.*, 1987], thereby verifying that similar electrical forces are occurring in the two beams.

Owing to the limitations of a one-dimensional simulation, we will not self-consistently model the overdense region of the beam very near the electron generator as was done by Winglee and Pritchett, but instead, we will model the beam after it has propagated $\sim 100\lambda_D$. In this region and beyond, the average beam density is considered less than that of the ambients. In a qualitative sense we can consider the modeling of the beam to start at point A labeled in Figure 3, where the average beam density is reduced and the beam temperature is still relatively cold.

Figures 4*a*, 4*b*, and 4*c* display the beam phase space config-

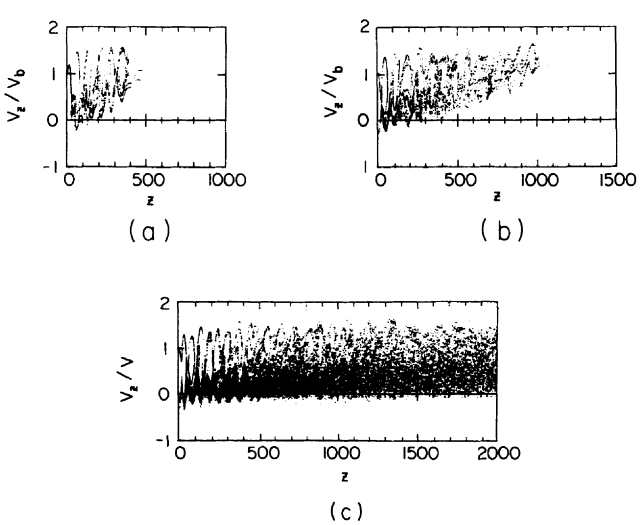

Fig. 4. Beam phase space configuration from our one-dimensional simulation after (*a*) $50\omega_{pe}^{-1}$, (*b*) $100\omega_{pe}^{-1}$ and (*c*) $840\omega_{pe}^{-1}$. In this simulation the beam model represents the underdense part of the beam displayed in Figure 3 starting from point A. The simulation was run with $n_b/n_A = 1/16$ and $V_b/V_A = 20$.

uration from our one-dimensional simulation after 50, 100, and $840\omega_{pe}^{-1}$, respectively. In this model, $n_b/n_A = 1/16$, $V_b/V_{TH} = 20$, and the beam is initially cold at $z = 0$. Each unit of distance represents $2\lambda_D$, or about 10 cm; thus Figure 4*c* displays the beam phase space configuration for a 200-m beam segment. The simulation was run for $840\omega_{pe}^{-1}$ to allow the transient front edge of the beam to leave the system. Consequently, the model displayed in Figure 4*c* represents the steady state beam. Note from the figures that the wave-particle trapping structures are similar to those of the two-dimensional beam displayed in Figure 3, implying that both are undergoing similar electrostatic interactions. Also note that the beam phase space configuration appears very similar to those modeled by *Okuda et al.* [1987], who performed a one-dimensional simulation similar to the one presented here. Figures 5*a*, 5*b*, and 5*c* display the number of beam particles as a function of z at times corresponding to those in Figure 4. Note from both Figures 4 and 5 that the beam is undergoing strong interactions with the background ionospheric medium. In the first 100 m ($z = 0$ to 1000), the beam-plasma instability is creating the classic trapping structures associated with such instabilities, which gives rise to significant perturbations in the density. Beyond 100 m ($z > 1000$), the beam is strongly thermalized, with the beam particles becoming randomized in phase space owing to the wave-particle interactions. Such randomization of the particles signifies the transfer of free energy from the beam to the electrostatic turbulence. Even though the beam becomes randomized, some significant density fluctuations are still present out past 100 m ($z > 1000$), as is indicated in Figure 5*c*.

According to expression (20) the current density of the beam is needed to obtain the radiated power. Figure 6*a* displays the beam current density, $J_z(z, t = 840\omega_{pe}^{-1})$, in the 200-m beam segment. Note from the figure that current density perturbations are clearly evident in the beam. It is the radiative coherence within and between these perturbations that yield significant wave powers, since the randomized background beam component only contributes to the incoherent power level. Figure 6*b* displays the Fourier transform of the current, $J_z(k_z)$, as a function of k_z. The resulting transform appears as a white noise type k spectra for $k_z > 20$; however, for $k_z < 20$, $J_z(k_z)$ appears to increase as k_z decreases. The white noise type k spectra found in $k_z > 20$ results from the randomized component of the electrons in the computer model. Although not feasible, if electrons with real mass and charge had been modeled, this noise would be significantly reduced. The average noise level was obtained by calculating the arithmetic average of the $J_z(k_z)$ values between 23.6 and 31.4. This level is represented by the line in Figure 6*b*. The increase in $J_z(k_z)$ found at $k_z < 20$ results from wave-particle interactions within the beam that create current density perturbations or "bunches." If bunching had not occurred, the simulated beam electrons would be completely randomized in phase space, and the resulting values of $J_z(k_z)$ would appear as white noise at all k_z values.

4. Radiated Power From a Model of the SL 2 Electron Beam

Equation (20) will now be applied to the simulated SL 2 electron beam discussed in the last section. In applying this expression to waves propagating in the SL 2 electron beam environment, some further approximations can be made. Specifically, in the frequency range of consideration, $n_1 \gg n_2$, $n_1 \simeq n$, where n is the whistler mode index of refraction obtained from cold plasma theory, and $T_{33}(n_1) \simeq 10^3\ T_{33}(n_2)$. Also, based on arguments of the typical density structure size in the beam, $J_z[k_z(n_2, \theta_0)] > J_z[k_z(n_1, \theta_0)]$. Consequently, the $k = 2$ term in the summation of (20) is very small and can be neglected. The radiated power can then be expressed as

$$P(t) = \bar{P} \simeq \int_{-\infty}^{\infty} \left[\frac{-|\omega|\, d\omega}{8\pi\varepsilon_0\varepsilon_1 c^2 V_s} \frac{1}{(n_2^2 - n_1^2)}\right] \cdot 2\pi J_z(k_z')J_z^*(k_z')T_{33}(n_1) \qquad (21)$$

where $k_z' = n \cos \theta_0 \omega/c$. Note that $n_1 > n_2$, which makes the term in brackets positive for the frequency range considered. To derive (21), it was assumed that a frame of reference exists where the current density is time independent, and thus all current density perturbations propagate at the same speed, V_s. In this case, the transform of the current density is properly represented by (11), where the delta function specifies the propagation speed V_s of the perturbations. In reality, however, all the perturbations may not be propagating at the same speed, and the validity of using (21) to estimate the coherent radiated power must be established. Consider a more realistic case where the density perturbations propagate with a speed $V \pm \Delta V$, where ΔV represents a velocity spread of the perturbations. In this case, the delta function in (11) should be replaced by a function that approximates this spread in velocity, such as a Gaussian function. As is demonstrated in the appendix, as long as this spread is not too great, the values of the radiated power are not significantly different from those obtained from perturbations all moving at identical velocities.

The velocity of the perturbations, V_s, must be determined in order to obtain a solution to (21). This velocity can be found by examining the spatial and temporal evolution of the current density perturbations in the simulation. By plotting the current density values above the average, $J_z(z, t) > 0.05$ A, as a function of z and t, the evolution of the individual perturbations can be followed. Such a plot is displayed in Figure 7. From this figure we see that the current density perturbations drift from the injection point at nearly the initial beam speed of 1.89×10^7 m/s. However, not all the perturbations move at the same identical speed, since at certain times, merging of a number of perturbations occurs. Examples of such current density enhancements are at $x = 100$ m, $t = 2.1 \times 10^{-5}$ s and at $x = 85$ m, $t = 3 \times 10^{-5}$ s and are circled in the figure. It is the creation of these structures coupled with the perturbations near the injection boundary that yield the large values of $J_z(k_z)$ at small wave numbers ($k_z < 0.2$) shown in Figure 6*b*. The Fourier transform of the current density, $J_z(k_z, \omega)$, is displayed in Figure 8. Note from this figure that the most intense values of the current corresponding to the perturbations lie near $V_s = 1.89 \times 10^7$ m/s, which is represented by the solid line in the figure. We also see that there is a spread in these values about V_s, but this spread is not very large and (21) can be readily applied. It is interesting to note that even though the beam itself develops a significant velocity spread, as indicated in Figure 4, the perturbations which generate significant radiation continue to propagate at the injection speed with little spread.

Recently, *Omura and Matsumoto* [1988] suggested that the bunches in their two-dimensional periodic beam simulation quickly reached a "quasi-linear phase" where they became "smoothed out," and thus significant radiation from these bunches could not occur. In the simulation presented here, we

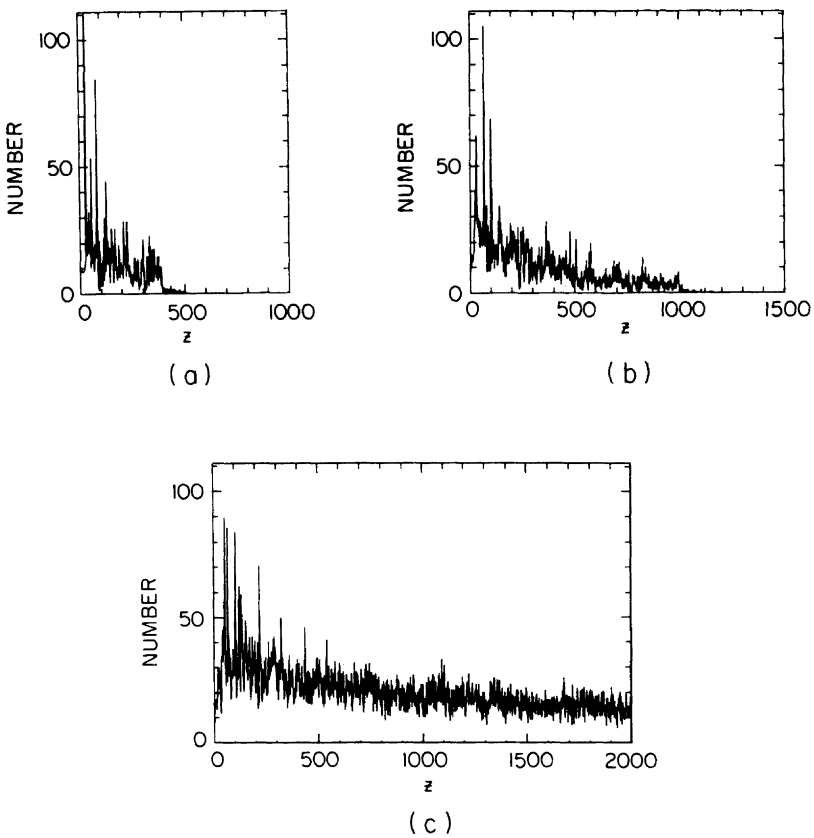

Fig. 5. Number of beam electrons as a function of z at times corresponding to those of Figure 4. Note from all three figures that significant density perturbations are created in the beam.

also see the bunches in the beam quickly reach this quasi-linear phase between 50 and 100 m from the injection point (see Figure 4). However, as is indicated in Figure 7, significant current density enhancements still exist out as far as 200 m, and these fluctuations affect the Cerenkov radiation. In particular, they couple to the strong perturbations found in the first 50 m, increasing the values of $J_z(k_z)$ in the whistler mode wave number regime (see Figure 6). This coupling effect is best mod-

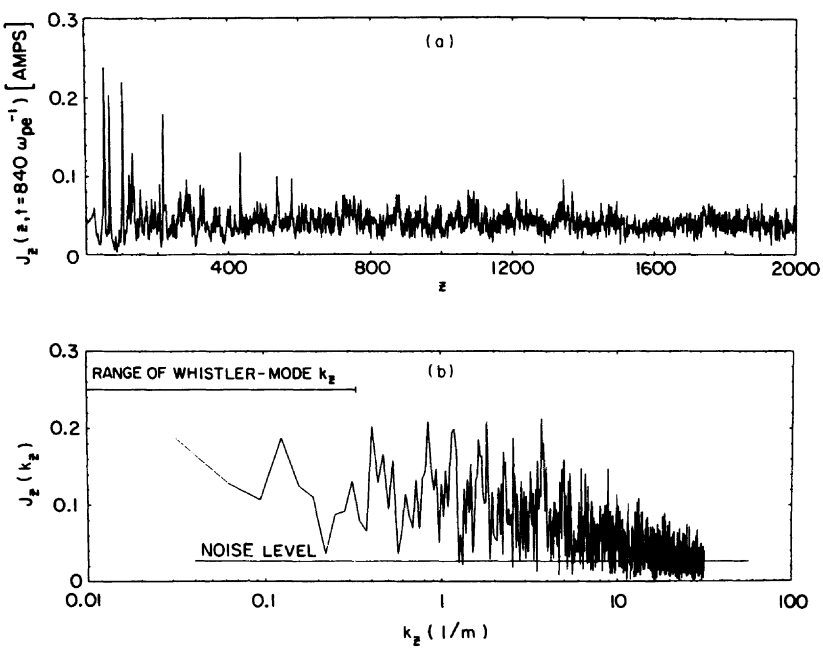

Fig. 6. Beam current density as a function of z at $840\omega_{pe}^{-1}$; (*b*) corresponding transform of this current. Note from Figure 6*a* that significant perturbations in the current density are present in the beam, which increases the values of $J_z(k_z)$ displayed in Figure 6*b* at wave numbers of less than 20.

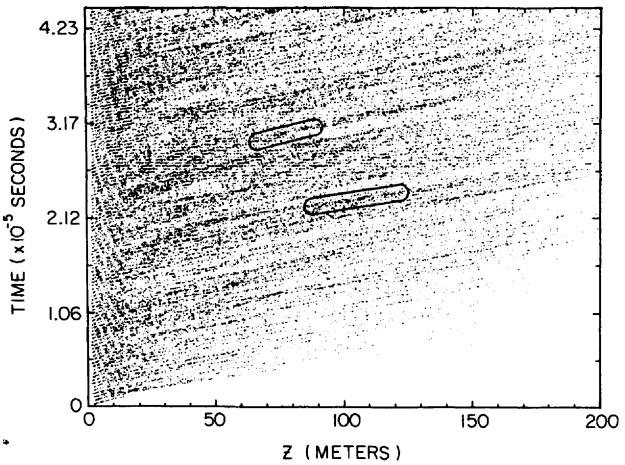

Fig. 7. Current density values, $J_z(z, t)$, above the average of 0.05 A as a function of z and t. The evolution of the current density perturbations is clearly displayed. Note that these perturbations drift at $V \sim 1.89 \times 10^7$ m/s, which is the beam injection speed. Also, note that merging of the current density perturbations occurs in the beam, as indicated by the circled structures.

eled using an injection simulation, which may possibly explain the different conclusions reached by *Omura and Matsumoto* [1988].

To obtain the radiated power from (21), $J_z(k_z)$ evaluated at $k_z'(\omega) = n \cos \theta_0 \omega/c$ is required, where the wave number $k_z'(\omega)$ represents those of the whistler mode that satisfy the Landau resonance condition. This wave number varies from 0.01 at 31.1 kHz to 0.332 at 1 MHz. The current density values that correspond to these wave numbers are indicated in Figure 6*b*. Using (21) and the calculated values of $J_z(k_z)$ with the noise level subtracted, the radiated power spectral density, dP/df, from the modeled 200-m beam segment is evaluated. These power spectral density values are plotted as a function of wave frequency in Figure 9 (represented by crosses), along with the log average of these values (represented by the straight line). The calculated incoherent Cerenkov power spectra (represented by open circles) and measured whistler mode power spectra (represented by dots) from the 200-m SL 2 electron beam segment is also displayed in the figure. Note from the figure that the inclusion of coherent effects among the beam electrons increases the wave powers by nearly a factor of 10^9 (90 decibels) above incoherent power levels and yields values that are relatively close to the measured whistler mode powers. It is clear from the figure that coherent Cerenkov radiation from the beam can indeed account for the measured whistler mode wave power.

It can also be seen from Figure 9 that the calculated power from the modeled beam actually overestimates the measured power by a factor of 40. This overestimate may result from the fact that the SL 2 electron beam is not an ideal line source radiator as assumed in our analysis, and a more accurate estimate of the power may be obtained by including the beam's radial dimension. The overestimate of the power may also be due to the assumption that the beam electrons are completely field aligned. Even if the electron generator is perfectly aligned with the geomagnetic field, electrical and fluid edge effects between the beam and the generator orifice may impart enough perpendicular momentum to the beam electrons to reduce the size of the density perturbations as we have modeled them. Consequently, the radiated power will be reduced. Interactions between the beam electrons and neutrals may also impart significant perpendicular momentum to the beam electrons, which will again reduce the size of the density perturbations and the radiated power. It might be expected that Landau damping of the Cerenkov radiation as it propagates in the ionospheric plasma will also reduce wave powers; but it is suspected that this effect is not significant, since the Cerenkov wave phase speed from the current density perturbations is still well above the thermal velocity of the ionosphere. On the basis of the limiting assumptions used in our model, the calculated power should be considered as an upper limit of the possible whistler mode wave power. The effects mentioned above should all tend to reduce the beam's radiative coherence as compared to our one-dimensional model and, consequently, lower the radiated powers. Therefore it is not surprising that the powers obtained via the one-dimensional analysis are higher than those measured.

5. CONCLUSION

Previously, the measured power of the whistler mode waves emitted by a continuous electron beam ejected from the shuttle was found to be almost 10^7 greater than the expected power from an incoherent Cerenkov radiation process. Owing to this discrepancy, it was suggested that these waves might result from coherent Cerenkov radiation effects in a beam naturally modulated by a beam-plasma instability. In this case, the enhanced radiated power would result from the coherence between electrons in the instability-related density perturbations or "bunches."

In order to verify that this process is indeed viable, a one-dimensional electrostatic simulation of the beam was performed that verified the existence of the bunches. The coherent Cerenkov-radiated power from the modeled beam was then calculated using an analytical expression similar to that pre-

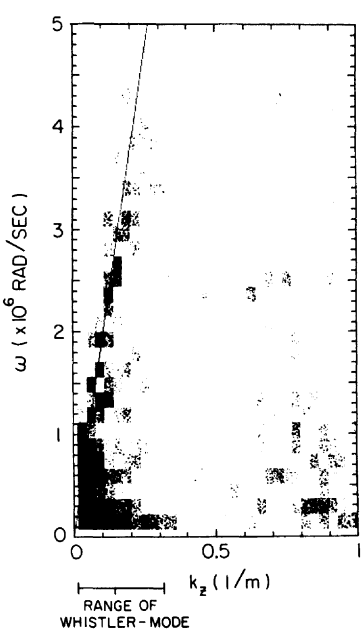

Fig. 8. To determine the velocity of the perturbations, the Fourier transform of the current density in time and space, $J_z(k_z, \omega)$, was calculated and plotted as a function of k_z and ω. Note that the values lie near $\omega/k_z = 1.89 \times 10^7$ m/s.

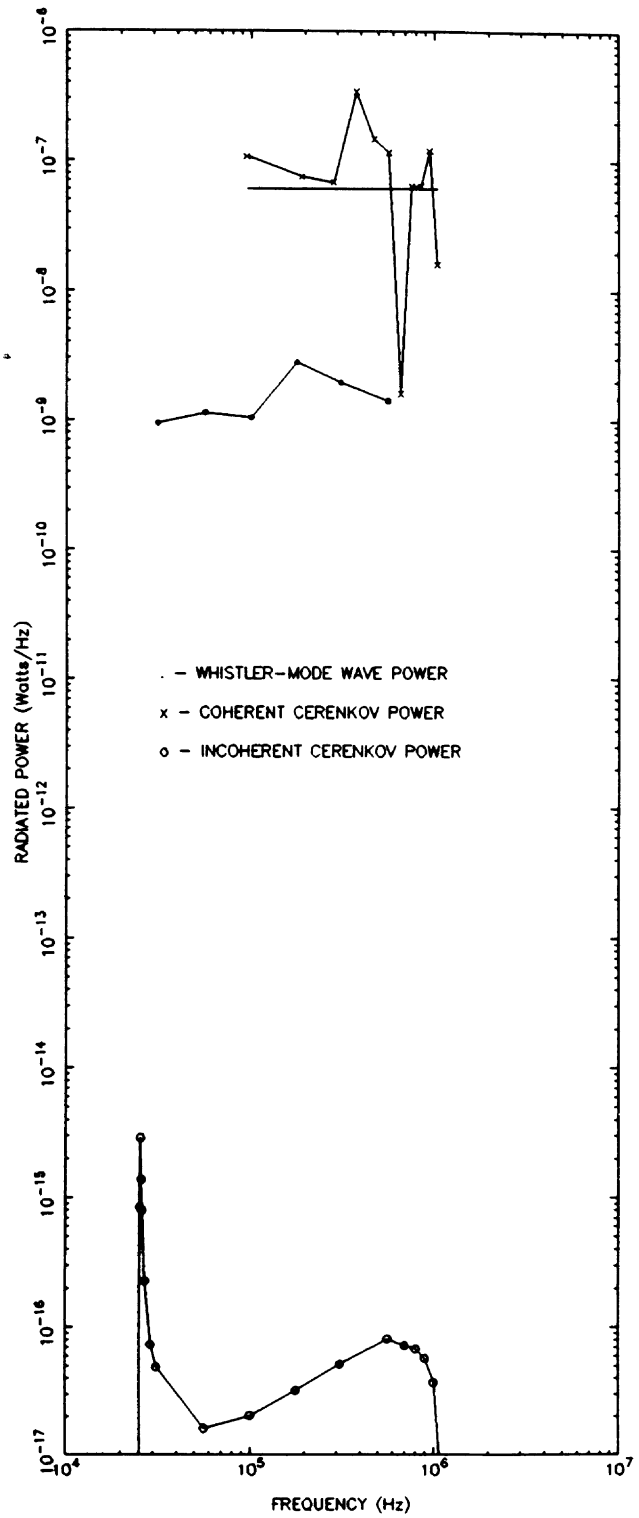

Fig. 9. Power spectra of the measured whistler mode radiation from the first 200 m of the SL 2 electron beam along with the calculated power spectra of the incoherent and coherent Cerenkov radiation from a 200-m beam segment. Note that the inclusion of coherent radiation effects increases the calculated powers near to those measured from the SL 2 electron beam. On the basis of these results, it is concluded that coherent Cerenkov radiation from a bunched electron beam can generate the detected whistler mode radiation.

sented by *Harker and Banks* [1983] and was found to be within a factor of 40 of the measured wave power.

It should be noted that two very critical assumptions were made to simplify the above analysis. The first assumption was that the beam could be treated as a line source radiator of the whistler mode waves and was invoked to obtain a manageable expression for the radiated power. Although the beam was not an ideal line source, the electromagnetic wavelengths were still significantly greater than the beam diameter, making the assumption valid. The second assumption is that similar electrostatic effects occur in beams of finite and infinite radius, which allowed us to model the beam using only a one-dimensional simulation. As was mentioned previously, a one-dimensional simulation was advantageous, since a long beam length was required. We demonstrated, via simulation, that the phase space structure of a two-dimensional, radially finite beam was indeed comparable to that of a one-dimensional beam. Without these two simplifying assumptions, the expression for the radiated power and the modeled beam could not have been used in the analysis.

Since we have demonstrated that a spontaneous emission process alone can account for the whistler mode wave powers, other more sophisticated emission processes operating in the beam, such as a whistler mode instability, are not required. Both a Cerenkov radiation process and a whistler mode instability could be present in the beam, but in this case, the powers from the Cerenkov process are at least comparable to those from the instability. Consequently, effects from spontaneous Cerenkov radiation processes cannot be ignored in the generation of the whistler mode waves from the SL 2 electron beam.

APPENDIX

As was mentioned in the text, all the current density perturbations or bunches in the modeled SL 2 electron beam are not propagating at exactly V_s but, instead, propagate in a range of velocities, $V_s \pm \Delta V$, where ΔV is the typical velocity spread. Consequently, in the frame moving with these bunches, they are not all stationary, as was assumed in the derivation of (21), but have second-order temporal variations that can alter the radiative coherence of the beam. The effect of these temporal variations on the radiated power can be accounted for by changing the delta function in (11) to a Gaussian function that represents the spread in bunch velocity. The corresponding transform of the current density in space and time is then written as

$$\bar{J}_q(\bar{k}, \omega) = \frac{\hat{z}}{(2\pi)^3} (2\pi)^{1/2} J_z(k_z) \left[\frac{t_0}{2(\pi)^{1/2}} e^{-a^2 t_0^2/4} \right] \qquad \text{(A1)}$$

where $J_z(k_z)$ is the spatial transform of the current density, $a = k_z V_s - \omega$, and t_0 is the typical coherence time scale of the temporal variations in the current density. If the transform of the current density is peaked at $\omega/k_z = V_s$ with little or no spread in ω or k_z, then the current density is properly represented by (11). However, as Figure 8 indicates, the transform of the current density, $J_z(k_z, \omega)$, has some spread about $V_s = \omega/k_z = 1.89 \times 10^7$ m/s. Consequently, this transform is best represented by (A1), where the Gaussian function is used to represent the spread in ω-k_z space. Note as $t_0 \rightarrow \infty$, (A1) and (11) become identical.

Following a similar analysis as was done previously, the power spectral density from a current density, $J_z(k_z, \omega)$, with a

spread is found to be

$$\left.\overline{\frac{dP}{d\omega}}\right|_{\omega=\omega_0} = \int F(k_z, \omega_0)\frac{t_0}{2(\pi)^{1/2}} e^{-a^2 t_0^2/4}\, dk_z \qquad \text{(A2)}$$

where

$$F(k_z, \omega_0) = \frac{1}{(2\pi)^2 \varepsilon_0 c^2}\int (\hat{z}\cdot \mathbf{T}^{-1}\cdot \hat{z})[2\pi J_z(k_z) J_z^*(k_z)] n\omega_0\, dn \qquad \text{(A3)}$$

Thus to obtain the power spectra density, a Gaussian-weighted integration of $F(k_z, \omega_0)$ over dk_z must be performed. Using (13), a similar expression can be written when $J_z(k_z, \omega)$ has no spread about $\omega/k_{\|} = V_s$:

$$\left.\overline{\frac{dP}{d\omega}}\right|_{\omega=\omega_0} = \int F(k_z, \omega_0)\delta(k_z V_s - \omega_0) e^{i(k_z V_s - \omega_0)t}\, dk_z$$

$$= \left.\frac{F(k_{z0}, \omega_0)}{V_s}\right|_{k_{z0}=\omega_0/V_s} \qquad \text{(A4)}$$

Expressions (A2) and (A4) should yield similar results as long as $F(k_z, \omega_0)$ approximates $F(k_{z0}, \omega_0)$ in dk_z. A numerical integration of (A2) was performed, and this result was indeed found to be true. The radiated power varied by only about 10% when considering a spread in $J_z(k_z, \omega)$ equal to k_{z0}. From these results it is evident that the radiated power does not vary significantly when considering a spread in $J_z(k_z, \omega)$ about $\omega/k_z = V_s$. Consequently, the radiated power calculated using the much simpler expression (21) should be a sufficiently accurate estimate of the radiated power from the modeled beam.

Acknowledgments. We would like to thank Terry Whelan and Shinobu Machida for their timely ideas concerning the simulation and radiated power calculations, John Steinberg for his useful discussions, Terry Averkamp for his valuable input on PDP data analysis, and John Birkbeck for a fine drafting job. Part of this research was funded by NASA graduate student researchers training grant NGT-50034. The research at the University of Iowa was also supported by NASA through contract 32807 and grants NAG3-449, NSG-7632, NGL 16-001-002, and NGL 16-001-043. The research at Stanford University was supported by NASA through grant NAGW-235.

The Editor thanks three referees for their assistance in evaluating this paper.

REFERENCES

Banks, P. M., and W. J. Raitt, Observations of electron beam structure in space experiments, *J. Geophys. Res.*, *93*, 5811, 1988.

Beghin, C., J. P. Lebreton, B. N. Maehlum, J. Troim, P. Ingsoy, and J. L. Michau, Phenomena induced by charged particle beams, *Science*, *225*, 188, 1984.

Bell, T. F., Artificial production of VLF hiss, *J. Geophys. Res.*, *73*, 4409, 1968.

Cartwright, D. G., and P. J. Kellogg, Observations of radiation from an electron beam artificially injected into the ionosphere, *J. Geophys. Res.*, *79*, 1439, 1974.

Dechambre, M., Yu. V. Kushnerevsky, J. Lavergnat, R. Pellot, S. A. Pulinets, and V. V. Seleger, Waves observed by the ARAKS experiment: The whistler mode, *Ann. Geophys.*, *36*, 351, 1980.

Farrell, W. M., D. A. Gurnett, P. M. Banks, R. I. Bush, and W. J. Raitt, An analysis of whistler mode radiation from the Spacelab 2 electron beam, *J. Geophys. Res.*, *93*, 153, 1988.

Gendrin, R., Initial expansion phase of an artificially injected electron beam, *Planet. Space Sci.*, *22*, 633, 1974.

Grandel, B. (Ed.), *Artificial Particle Beams in Space Plasma Studies*, Plenum, New York, 1982.

Gurnett, D. A., A satellite study of VLF hiss, *J. Geophys. Res.*, *71*, 5599, 1966.

Gurnett, D. A., High latitude electromagnetic plasma wave emissions, in *High Latitude Space Physics*, edited by B. Hultqvist and T. Hagfors, Plenum, New York, 1983.

Gurnett, D. A., W. S. Kurth, J. T. Steinberg, P. M. Banks, R. I. Bush, and W. J. Raitt, Whistler-mode radiation from the Spacelab-2 electron beam, *Geophys. Res. Lett.*, *13*, 225, 1986.

Harker, K. J., and P. M. Banks, Radiation from pulsed electron beams in space plasmas, *Radio Sci.*, *19*, 454, 1983.

Hawkins, J. G., P. M. Banks, P. R. Williamson, R. I. Bush, and W. J. Raitt, Rise times in the vehicle charging and return current measurements during electron beam emission experiments from the shuttle orbiter (abstract), *Eos Trans. AGU*, *68*, 1400, 1987.

Lin, C. S., and H. K. Wong, Plasma instabilities of a finite size electron beam-plasma system, paper presented at 1988 URSI Meeting, Union Radio Scientifique Internationale, Boulder, Colo., 1988.

Lin, C. S., J. L. Burch, S. D. Shawhan, and D. A. Gurnett, Correlation of auroral hiss and upward electron beams near the polar cusp, *J. Geophys. Res.*, *89*, 925, 1984.

Mansfield, V. N., Radiation from a charged particle spiraling in a cold magnetoplasma, *Astrophys. J.*, *147*, 672, 1967.

Monson, S. J., P. J. Kellogg, and D. G. Cartwright, Whistler mode plasma waves observed on Electron Echo 2, *J. Geophys. Res.*, *81*, 2193, 1976.

Neubert, T., W. W. L. Taylor, L. R. O. Storey, N. Kawashima, W. T. Roberts, D. L. Reasoner, P. M. Banks, D. A. Gurnett, R. L. Williams, and J. L. Burch, Waves generated during electron beam emissions from the space shuttle, *J. Geophys. Res.*, *91*, 11,321, 1986.

Okuda, H., and J. D. Kan, Injection of an electron beam into a plasma and spacecraft charging, *Phys. Fluids*, *30*, 209, 1987.

Okuda, H., R. Horton, M. Ono, and M. Ashour-Abdalla, Propagation of a nonrelativistic electron beam in a plasma in a magnetic field, *Phys. Fluids*, *30*, 200, 1987.

Omura, Y., and H. Matsumoto, Computer experiments on whistler and plasma wave emissions for Spacelab-2 electron beam, *Geophys. Res. Lett.*, *15*, 319, 1988.

Shawhan, S. D., G. B. Murphy, P. M. Banks, P. R. Williamson, and W. J. Raitt, Wave emissions from dc and modulated electron beams on STS 3, *Radio Sci.*, *19*, 471, 1984.

Williamson, P. R., J. G. Hawkins, R. I. Bush, P. M. Banks, and W. J. Raitt, Vehicle charging measured during electron beam emission on Spacelab-2 (abstract), *Eos Trans. AGU*, *66*, 1051, 1985.

Winglee, R. M., and P. L. Pritchett, Comparative study of cross-field and field-aligned electron beams in active experiments, *J. Geophys. Res.*, *93*, 5823, 1988.

Winglee, R. M., P. L. Pritchett, and G. A. Dulk, Energy transport by energetic electrons released during solar flares, 1, Thermal versus nonthermal processes, *Astrophys. J.*, in press, 1987.

W. M. Farrell, C. K. Goertz, and D. A. Gurnett, Department of Physics and Astronomy, G375, University of Iowa, Iowa City, IA 52242.

(Received October 27, 1987;
revised July 22, 1988;
accepted July 26, 1988.)